Structural Safety 73 (2018) 54–63

Contents lists available at ScienceDirect

Structural Safety

journal homepage: www.elsevier.com/locate/strusafe

Methodology for real-time prediction of structural seismic risk based on sensor measurements

Ajay Saini *, Iris Tien

School of Civil and Environmental Engineering, Georgia Institute of Technology, Atlanta, GA 30332-0355, USA

ARTICLE INFO

Article history:
Received 22 August 2016
Received in revised form 15 September 2017
Accepted 19 February 2018

Keywords:
Structural seismic risk
Probabilistic inference
Maximum response prediction
Sensor measurements
Ground motion simulation
Earthquake early warning

ABSTRACT

Current earthquake early warning systems utilize p-wave data to predict the extent of an earthquake threat and issue warnings at a regional scale. In the assessment of seismic risk, we propose a methodology to go beyond ground motion prediction to consider the response of the structure itself. It is a localized real-time approach where we utilize the first 3 s of data from sensors mounted on a structure to infer the characteristics of the upcoming earthquake. These parameters are used to simulate ground acceleration histories and the structural response estimated under each input motion. A structure-specific warning can then be issued based on the predicted maximum structural response. The method enables probabilistic inference on the structural risk to the earthquake event. In this paper, we describe the proposed methodology and apply it to an example earthquake. We assess the accuracy of the method, compute its computational efficiency, and investigate its robustness to uncertainty in system parameters. Finally, we apply the method to several recorded earthquakes to demonstrate its generalizability. The approach does not require extensive knowledge of regional earthquakes or site characteristics. Such data, however, if available, can be easily incorporated to improve the efficiency and accuracy of the method.

Published by Elsevier Ltd.

1. Introduction

Earthquakes are among the most significant natural hazards we face, causing an average of $12 billion in economic damages and nearly 13,000 deaths annually across the globe [1]. The risk from any natural hazard depends on the occurrence and extent of the hazard, vulnerability of the infrastructure, and consequential effects on the population. With aging infrastructure, growing populations in earthquake-prone areas, and an increasing number of earthquakes including due to human activities such as fracking and saltwater disposal, global seismic risk is increasing. Effective earthquake early warning systems would enable protective measures to be taken and vulnerable populations to seek safety before the full extent of a seismic event occurs.

The complexity in the nucleation and growth of an earthquake, however, makes it difficult to accurately predict seismic events. Recently, several early warning systems have been developed, which use real-time seismology to issue an earthquake warning, e.g. Earthquake Early Warning (EEW) program run nationwide in Japan by Japan Meteorological Agency (JMA), ShakeAlert early warning system operated in California through California Integrated Seismic Network (CISN), and Seismic Alert System (SAS) running in Mexico City. These systems rely on the real-time recording and processing of earthquake data. Such models predict the extent of a regional earthquake threat based on the content of the seismic wave within the initial few seconds of a recorded event. We propose an early warning system that goes beyond ground motion prediction to consider the response of the structure itself. The objective is to create a methodology that provides an earthquake early warning based on the anticipated structural response, which is predicted from information from sparsely instrumented buildings rather than relying on extensive seismological data. The proposed localized and structure-specific approach uses collected data to run simulations and create a suite of synthetic accelerograms. These accelerograms are then used to estimate structural responses, with warnings based on predicted maximum responses.

Specifically, the methodology first takes the data from an accelerometer placed on the structure and separates the ground motion and structural response in real time. The initial 3 s of p-wave data is used to estimate the characteristics of the earthquake, including moment magnitude, Arias intensity, and hypocentral distance from the structure. A number of ground motions are then simulated based on these parameters. From these, we find the structural response for each simulated ground motion and infer the maximum structural response due to the upcoming earthquake. The future structural response is predicted as the average

* Corresponding author.
E-mail addresses: ajaysaini@gatech.edu (A. Saini), itien@ce.gatech.edu (I. Tien).

https://doi.org/10.1016/j.strusafe.2018.02.004
0167-4730/Published by Elsevier Ltd.

of the responses to the set of predictive simulated ground motions. The proposed method does not require extensive knowledge of the regional seismic history, local ground characteristics, or information from additional seismograph stations. It is a minimalist approach, which can, however, be made more accurate if conditioned on additional known seismological information at the site under consideration.

The rest of the paper is organized as follows: Section 2 provides background on previous work on seismic risk and earthquake early warning systems. Section 3 describes the proposed methodology, including separation of the ground motion and structural response, early prediction of earthquake parameters, and simulation of ground motions. The results of the methodology are presented in Section 4, with the distribution of predicted maximum responses and root mean square errors of the predictions presented for an example earthquake. Computational efficiency of the methodology is investigated, as well as robustness of the method to uncertainty in assumed system parameters. Finally, the methodology is applied to several earthquakes to investigate the generalizability of the methodology across earthquake events.

2. Background

Most of the previous work on structural seismic risk has focused on assessing risk to a building or region before or after an event has occurred. Pre-event analyses include recent work in response estimation and building portfolio reliability assessment to compute seismic loss probabilities [2–3]. Other work includes quantifying uncertainty in seismic risk assessment [4] and risk assessment for particular structures, such as reinforced-concrete frames [5–6], seismically isolated structures [7], and bridges [8]. Post-event analyses focus on damage mapping [9] and assessment [10] after the earthquake has occurred. In contrast to these studies, the methodology proposed here is for real-time prediction of seismic risk given the occurring ground motion. This is related to previous work in earthquake early warning with a focus on structural response in particular.

The development of earthquake early warning systems using real-time seismology dates back to Nakamura's introduction to the concept of using frequency content of p-waves for inferences on the characteristics of an earthquake [11]. The frequency content in the initial few seconds of the p-wave can be analyzed either as the period of a monochromatic wave (τ_c) or as the maximum period (τ_p^{max}). Kanamori [12] extended Nakamura's work to use in practical real-time seismology. Studies by Wu and Kanamori [13–16] show a strong correlation between τ_c and moment magnitude M_w. They developed an early warning system based on the initial 3 s of the p-wave by observing τ_c and the maximum ground displacement P_d. Through the τ_c - P_d method, P_d was found to have a good correlation with the peak ground velocity (PGV) of the approaching earthquake. Allen and Kanamori [17] and Olson and Allen [18] used τ_p^{max} to develop a similar methodology. Through the τ_p^{max} - P_d method, their work shows a strong relationship between τ_p^{max} and M_w.

Wurman, Allen, and Lombard [19]; Allen [20]; and Allen et al. [21] proposed ElarmS, which uses a network-based approach. It extends the single station approach from previous studies to a network of stations, where the data from the entire network is processed simultaneously to issue a regional warning. Cua and Heaton [22] developed virtual seismologist (VS), using a Bayesian approach to predict the most probable magnitude and location of an earthquake given observations through conditioning on historical data. An extensive data history is required for the prior distributions and conditioning. Wu, Kanamori, Allen, and Hauksson, [23]; and Shieh, Wu, and Allen [24] found relationships between the initial ground motion parameters and earthquake characteristics, with these methods subsequently used for earthquake warning applications in Böse, Hauksson, Solanki, and Kanamori [25]; Böse, Heaton, and Hauksson [26]; and Cheng, Wu, Heaton, and Beck [27].

All of the described earthquake early warning systems predict the extent of an upcoming earthquake for a region. These methods do not account for the behavior of individual structures. Assessing the seismic risk for a particular building requires a combined analysis of the ground motion and structural behavior. Therefore, we move beyond regional earthquake warnings to create a structure-specific and localized earthquake early warning system. This study investigates our proposal that from the first 3 s of structural sensor data, we can obtain predictive characteristics of the earthquake. If we then simulate a number of ground motions, then the average structural response will conform to the actual response of the structure under the approaching earthquake, enabling an early warning to be issued.

3. Methodology

3.1. Flowchart

The full methodology is shown in the flowchart given in (Fig. 1). The specific steps of the process are described in detail in the following sections.

3.2. Separation of ground motion and structural response

In this study, we assume a minimally instrumented building using low-cost accelerometers. The first step of the process is to use the data from the accelerometers placed on the structure to obtain the ground motion signal. If the accelerometer is placed on the ground at the structure, then it captures the ground motion directly, but if the same sensor is placed on any other part of the structure, then it records the sum of the ground motion and the structural response. Therefore, we need to separate these two elements from the accelerometer measurements [28]. To do this, the unscented Kalman filter (UKF) is used as in [29]. In addition, the sensor recordings contain ambient noise. As shown in [30], the error in the estimate due to ambient noise reduces significantly if the sensor is placed on the higher stories of a structure. Hence, if a structure is instrumented with a single accelerometer, as is assumed in this study, we recommend that the sensor be placed on the top story of the building for these applications. The effect of ambient noise and uncertainty in structural parameters are studied in [29–30] and the methodology is shown to perform well even under high uncertainties. Therefore, separate terms for different uncertainties are not considered in this analysis.

To separate the ground motion from the structural response, we begin with the equation of motion for a structure subjected to ground acceleration

$$\mathbf{M}\ddot{\mathbf{u}}_{\mathbf{s}} + \mathbf{C}\dot{\mathbf{u}}_{\mathbf{s}} + \mathbf{F}(\mathbf{u}_{\mathbf{s}}) = -\mathbf{M}\mathbf{1}a_g \tag{1}$$

where $\mathbf{M}$, $\mathbf{C}$ and $\mathbf{F}$ represent the mass, damping and spring force matrices, respectively. $\mathbf{u}_{\mathbf{s}}$ represents displacement of the structure and a_g acceleration of the ground. Defining $\mathbf{z}^{\mathrm{T}} := [\mathbf{u}_{\mathbf{s}}^{\mathrm{T}} \;\; \dot{\mathbf{u}}_{\mathbf{s}}^{\mathrm{T}}]$ in first-order form, the equation of motion is

$$\dot{\mathbf{z}} = \begin{bmatrix} \mathbf{0} & \mathbf{I} \\ \mathbf{0} & -\mathbf{M}^{-1}\mathbf{C} \end{bmatrix}\mathbf{z} + \begin{bmatrix} \mathbf{0} \\ -\mathbf{M}^{-1}\mathbf{F}(\mathbf{z}) \end{bmatrix} + \begin{bmatrix} \mathbf{0} \\ -\mathbf{1} \end{bmatrix} a_g \tag{2}$$

$$\dot{\mathbf{z}} = \mathbf{A}_{\mathbf{c}}(\mathbf{z}) + \mathbf{b}_{\mathbf{c}} a_g \tag{3}$$

We discretize Eq. (2) as in [29] to obtain the evolution of the system from time step k to $k+1$

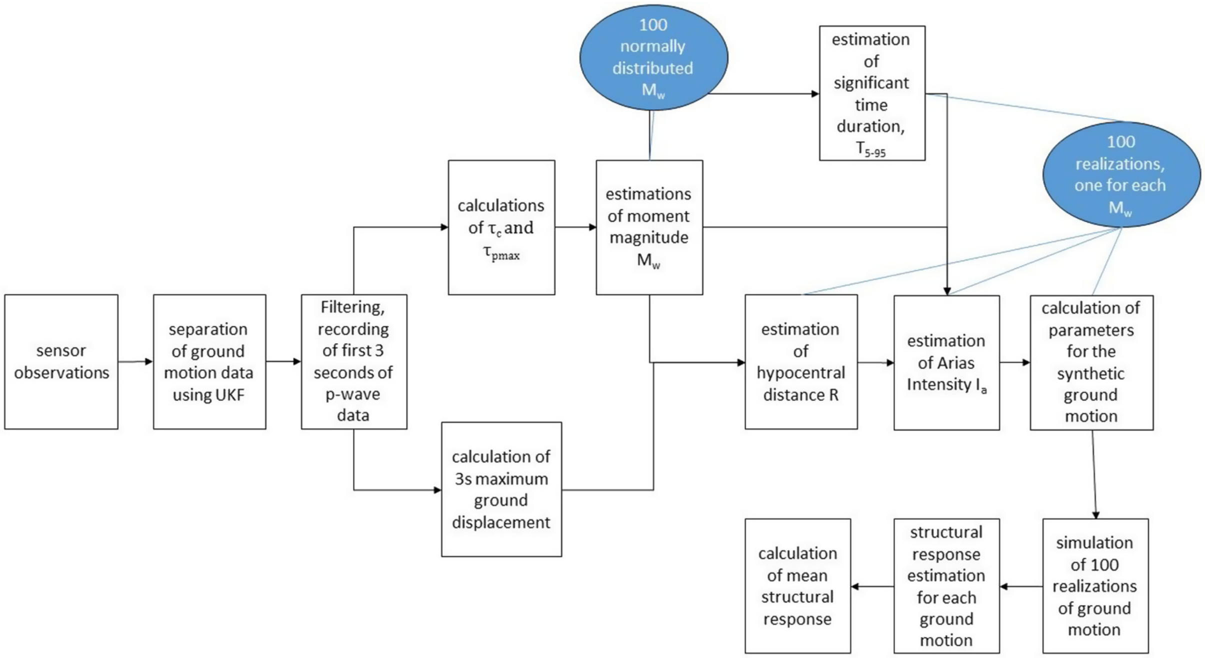

Fig. 1. Flowchart of the methodology.

$$\mathbf{z}_{k+1} = \mathbf{A_1}\mathbf{z}_k + \mathbf{F_1} + \mathbf{b}a_g \tag{4}$$

where

$$\mathbf{A_1} = \begin{bmatrix} \mathbf{I} & \mathbf{I}\Delta t \\ \mathbf{0} & e^{-\mathbf{M}^{-1}\mathbf{C}\Delta t} \end{bmatrix}$$

$$\mathbf{F_1} = \begin{bmatrix} \mathbf{0} \\ \mathbf{C}^{-1}\left(e^{-\mathbf{M}^{-1}\mathbf{C}\Delta t} - \mathbf{1}\right)\mathbf{F}(\mathbf{z}) \end{bmatrix}$$

$$\mathbf{b} = \frac{\mathbf{b_c}\left(e^{-2\xi_g\omega_g\Delta t} - 1\right)}{-2\xi_g\omega_g}$$

ξ_g and ω_g are the effective damping ratio and predominant angular frequency of the ground, respectively, Δt is the discretization time step, $\mathbf{b_c}$ is as defined in Eq. (3), $\mathbf{I}$ is the identity matrix, and 1 is a matrix with all elements being 1. Equation (4) shows the propagation of the system state in time. Using the UKF framework enables us to estimate the relative structural response $\mathbf{u_s}$ and $\dot{u}_\mathbf{s}$at every time step. The UKF framework initially extrapolates the response at the next time step using the response at the previous time step. The extrapolated response is then updated by accelerometer measurements to estimate the structural response at the current time step. The time step used throughout is the sampling time of the accelerometer.

Now, we define the structural acceleration a_{snk} as approximated using the UKF framework

$$a_{snk} = \frac{\ddot{u}_{snk+1} - \ddot{u}_{snk}}{\Delta t} \tag{5}$$

where subscript n represents the nth level where the accelerometer is placed, and subscript k indicates the kth time step. We use this structural acceleration to calculate the ground acceleration as

$$a_g = a_{tn} - a_{snk} \tag{6}$$

where a_{tn} is the total acceleration measured by the sensor placed at the nth story. From Eq. (6), the ground acceleration and relative structural acceleration are separated from the measured observations of the accelerometers.

As it is processed, the ground motion data is simultaneously passed through a 2-pole, 0.075-Hz Butterworth filter. The first 3 s of the filtered ground motion p-wave acceleration data is recorded for further analysis and inference. The data is also simultaneously integrated recursivel τ_c y to obtain the ground velocity and displacement response history. As with other EEW systems, it is assumed that the initial wave arrival corresponds with p-wave accelerations. If the distance between the investigated structure and the seismic hypocenter is short, this assumption may not hold. For a structure some distance from the earthquake hypocenter, however, this results in a warning time between a few seconds to 60+ seconds.

3.3. Inferences from first 3 s of p-wave data

The processed data for the first 3 s of the earthquake contains significant information about the seismic event. The measure of the frequency content of the recorded data is closely related to the intensity of earthquake. The peak ground displacement combined with the frequency content provide a good estimate of the hypocentral distance of the earthquake from the place of interest. There are two parameters used to measure the frequency content of the earthquake: [13–16] and τ_{pmax} [17–21].τ_c is a measure of the average period of ground motion or the period of the monochromatic wave. We first compute the moment rate function given as

$$r = \frac{\int_0^{\tau_0} \dot{u}^2(t)dt}{\int_0^{\tau_0} u^2(t)dt} \tag{7}$$

where τ_0 is 3 s from the onset of p-wave arrival, $\dot{u}(t)$ is the ground motion velocity, and $u(t)$ is ground motion displacement. Parseval's theorem suggests that

$$r = \frac{4\pi^2 \int_0^{\infty} f^2 |\hat{u}(f)|^2 df}{\int_0^{\infty} |\hat{u}(f)|^2 df} = 4\pi^2 < f^2 > \tag{8}$$

where f is the frequency, $\hat{u}(f)$is the frequency spectrum of $u(t)$ and $< f^2 >$ is the average of f^2 weighted by $|\hat{u}(f)|^2$. Combining the moment rate function and Parseval's theorem gives

$$\tau_c = \frac{1}{\sqrt{<f^2>}} = \frac{2\pi}{\sqrt{r}} \tag{9}$$

τ_p^{max}, unlike τ_c, is not the average period with respect to the frequency content of the wave. Rather, it is the dominant period of the wave in the period under consideration. τ_p is determined recursively as a time series from the waveform. It contains the information about the frequency content of the seismic waveform up to the time at which it is calculated. Therefore, we calculate τ_p at every time step and the maximum of τ_p during the 3 s is τ_p^{max}. τ_p is calculated as

$$\tau_{p_k} = 2\pi\sqrt{\frac{X_k}{D_k}} \tag{10}$$

where k corresponds to the kth time step and

$$X_k = \alpha X_{k-1} + \dot{u}_k^2 \tag{11}$$

$$D_k = \alpha D_{k-1} + \left(\frac{d\dot{u}}{dt}\right)_k^2 \tag{12}$$

where $\dot{u}_k$ is the velocity at the kth time step and α is a smoothing constant taken to be 0.99. The calculations for τ_p are started at t = 0.05 s rather than t = 0.00 s to avoid any error due to noise before the arrival of the p-wave in the recursive formulation.

The peak ground displacement (PGD) in the first 3 s is an important parameter as it correlates with the final peak ground velocity and hypocentral distance. Hence, we also record the PGD P_d contained in the first 3 s of the p-wave calculated from the integration of the separated ground motion acceleration signal.

3.4. Early prediction of earthquake parameters

The measured frequency content of the early p-wave is correlated to the moment magnitude of the earthquake. Although no direct relationship has been established, several empirical studies relate moment magnitude to the parameters calculated above. We use the results of these studies together to estimate a nominal mean moment magnitude M_w for the earthquake. The following empirical relations taken from the corresponding references are used: [24,16,23,20,18,19]

$$M_w = (\tau_c + 7.76)/1.56 \tag{13}$$

$$M_w = (\log_{10}\tau_c + 1.462)/0.296 \tag{14}$$

$$M_w = 4.218 * \log_{10}\tau_c + 6.1666 \tag{15}$$

$$M_w = 6.3 * \log_{10}\tau_p^{max} + 7.1 \tag{16}$$

$$M_w = 7 * \log_{10}\tau_p^{max} + 5.9 \tag{17}$$

$$M_w = \{(0.36 * \log_{10}PGA - 0.93 * \log_{10}P_d) - 5.495\}/(-0.615) \tag{18}$$

where PGA and P_d are peak ground acceleration and displacement, respectively, for the initial p-wave data.

From the above relations, we calculate the mean and standard deviation of the estimated moment magnitude of the earthquake using the approximations from each of the empirical relations. Due to uncertainty in this estimation and differences among the empirical relations, we create an array of 100 realizations of the moment magnitude for this earthquake by drawing randomized normally distributed values about the mean with the calculated standard deviation.

The next step is to predict the earthquake parameters: hypocentral distance R, significant duration t_{5-95}, and Arias intensity I_a. We predict the hypocentral distance R (km) from the site of interest based on the frequency content of the seismic wave and the PGD during the recorded 3 s. The empirical relation relating the hypocentral distance to the PGD (cm) and moment magnitude is [23]

$$\log_{10}R = \frac{M_w - 4.748 - 1.371 * \log_{10}P_d}{1.883} \tag{19}$$

Note that M_w is now an array of 100 realizations. Therefore, we obtain an array of 100 values for R corresponding to each realization of moment magnitude.

The significant time duration t_{5-95}, defined as the time occurring between 5% and 95% of Arias intensity, is related to the moment magnitude and hypocentral distance. There are three possible relations, given in Eqs. (20)(22), which can be used to find t_{5-95} with respect to each moment magnitude realization [31,32,33]

$$t_{5-95} = 0.02\exp(0.74M_w) + 0.3R \tag{20}$$

$$t_{5-95} = 11.2M_w - 53 \tag{21}$$

$$\log_{10}t_{5-95} = -1.3877 + 0.2451 * M_w + 0.6280 * \log_{10}\sqrt{4.5^2 + R^2} \tag{22}$$

Equation (21) works well only for $M_w > 6$ [32]. As an objective of this study is to create an automated system for earthquake early warning that is applicable across magnitudes of earthquake events, this relation is not used. We have found Eqs. (20) and (22) to produce similar results. However, Eq. (22) is more computationally expensive. Therefore, Eq. (20) is used in this study. It is noted that unlike M_w, the precise value of t_{5-95} does not significantly affect the outcome of the simulated ground motion. Therefore, while all 6 empirical relations are used to estimate M_w, and the mean and standard deviation of the result used for subsequent sampling, only one relation is used here. The result of this step is an array of 100 values for t_{5-95}.

Arias intensity depends on the acceleration content of the seismic waveform. In general, the Arias intensity of an earthquake is calculated as the sum of Arias intensities of the motion in both horizontal directions, i.e., $I_h = I_{EW} + I_{NS}$. In this study, we estimate the total horizontal Arias intensity based on moment magnitude, hypocentral distance, and soil class [34]. However, we need the Arias intensity specific to the dominant direction. We approximate the predominant Arias intensity to be a mean 60% of the total horizontal intensity [35]. Equation (23) gives the Arias intensity for each site class multiplied by a randomized factor k sampled from a truncated normal distribution with mean 0.6 and varying between 0.5 and 0.7 with standard deviation 0.1. $\in$ is a random error normally distributed with zero mean and specified standard deviation.

$$\text{Soil class}B\ I_a = k * \exp(2.071M_w - 2.178\ln R - 8.492 + (0, 1.29)) \tag{23-1}$$

$$\text{Soil class}C\ I_a = k * \exp(2.290M_w - 1.245\ln R - 13.539 + (0, 1.23)) \tag{23-2}$$

$$\text{Soil class}D\ I_a = k * \exp(2.155M_w - 1.323\ln R - 11.920 + (0, 1.25)) \tag{23-3}$$

$$\text{Soil class}E\ \ I_a = k * \exp(1.746M_w - 1.585\ln R - 7.409 + (0, 0.82)) \tag{23-4}$$

Thus, we estimate the Arias intensity for the predominant direction for different site classes. However, if the site class is unknown, then conservatively site class D may be used. In this study, for a general structure situated on a site, we have assumed the site class to be D. If further information is available about the site of interest, the relation for that particular site class may be used. The result from this step is an array of 100 values of Arias intensity.

3.5. Simulation of ground motions

Next, we simulate synthetic ground motions using the predicted earthquake parameters. This is done by modulating a normalized white noise process in time as in [36–37]. We choose a gamma modulating function given as

$$q(t,\boldsymbol{\alpha}) = \alpha_1 t^{\alpha_2-1}\exp(-\alpha_3 t) \tag{24}$$

where $q(t,\alpha)$ is the time-modulating function, t is time, and, $\boldsymbol{\alpha} = (\alpha_1, \alpha_2, \alpha_3)$ are the parameters controlling the properties of the function. α_1 controls the intensity of the process, α_2 the shape, and α_3 the duration of the motion. We use Arias intensity I_a, significant duration t_{5-95}, and the time of occurrence of the maximum shaking t_{mid} defined as the time of 45% Arias intensity to calculate the parameters of the modulating function.

We estimate the total period of the seismic motion as 3 times the significant duration [34]. The maximum intensity of an earthquake typically occurs during the initial phase with a longer right-side tail. Therefore, we factor the total time by a randomized factor normally distributed about a mean of 3 with standard deviation 0.5 to estimate t_{mid}. Now, we calculate $\boldsymbol{\alpha}$ as

$$\alpha_3 = \frac{1}{-\frac{t_{mid}}{2} + \frac{1}{4}\sqrt{4t_{mid}^2 + t_{5-95}^2}} \tag{25-1}$$

$$\alpha_2 = t_{mid} * \alpha_3 + 1 \tag{25-2}$$

$$\alpha_1 = \sqrt{I_a \frac{(2\alpha_3)^{2\alpha_2-1}}{\Gamma(2\alpha_2-1)}} \tag{25-3}$$

We estimate the impulse response function (IRF) of the filter as the pseudo acceleration response of a single degree of freedom linear oscillator as

$$h(t-\tau,\tau) = \begin{cases} \frac{\omega_f(\tau)}{\sqrt{1-\zeta_f^2}}\exp[-\zeta_f\omega_f(\tau)(t-\tau)] * \sin\left[\omega_f(\tau)\sqrt{1-\zeta_f^2}(t-\tau)\right] & \tau \leqslant t \\ 0 & otherwise \end{cases} \tag{26}$$

where t is the time at the kth step under consideration, and both t and τ range from 0 to the total time duration.

We approximate the filter frequency ω_f and filter damping ratio ζ_f using the count of zero-level up-crossings [32]. We count the cumulative number of zero-level up-crossings at each time step during the recorded 3 s of motion and find the best second-order curve-fit approximation for it. The slope of the curve gives ω_f as a function of time. We are assuming ζ_f to be independent of time. It is estimated using the cumulative count of positive minima and negative maxima in the recorded motion compared to the count for a target accelerogram of the same duration for ζ_f values between 0.1 and 0.9. We assume the directional components of the ground motion to be correlated to follow the same trend.

The discretized model for the ground acceleration a_g is given as

$$a_g(t) = q(t,\alpha) * \sum_{i=1}^{k-1}\{s_i(t,t_i)w_i\} \tag{27}$$

where

$$s_i(t,t_i) = \frac{h(t-t_i,t_i)}{\sqrt{\sum_{j=1}^{k} h^2(t-t_j,t_j)}} \tag{28}$$

k is chosen such that $t_k = t$ and w represents zero-mean white noise. We note that this simulation process slightly overestimates the response over the period of the seismic event, and it should be passed through a high-pass filter. However, we use the original simulation result as the ground acceleration in this study to be conservative in the estimation. From this process, we obtain 100 sets of time histories of the ground motion, corresponding to the 100 sets of estimated earthquake parameters. We are then able to predict the maximum structural response for each simulated ground motion using Eq. (4).

4. Results

We apply the proposed methodology to a single degree of freedom lumped mass system to estimate the maximum displacement response of a cantilever 12′ W10X49 column under an example earthquake event. The coefficient of damping is assumed to be 5%. The ground motion used is the Chi-Chi earthquake because of the availability of consistent high-resolution data across stations for this event. Results for the application of the proposed methodology to other earthquakes are provided later in this section. In this section, we present results on the efficiency of the proposed method in terms of number of simulations and computational time, assess the estimation accuracy of the method, provide probabilistic inference on structural risk to the earthquake event, and investigate robustness of the prediction to variation in system parameters. All the computations are performed in MATLAB R2015a on a Windows desktop computer with 8 GB RAM and 3.60 GHz processor.

4.1. Application of methodology to Chi-Chi earthquake

We first identify the parameters ω_f and ζ_f for the ground motion simulation. To estimate ω_f, we count the cumulative number of zero-level up-crossings as described in Section 3 and curve fit this as a second-order polynomial approximation. Its differential gives a first-order polynomial that represents ω_f varying in time.

To estimate ζ_f, we compare the cumulative number of positive minima and negative maxima of the ground motion with that of simulated accelerograms using different values of ζ_f. As the estimation of ζ_f is based on a cumulative count, a full time history is required to produce a reliable estimate of ζ_f [32]. Damping ratio is a ground property and we treat it as a constant predicted from any known ground motion time history at the site. Fig. 2 shows the cumulative count of positive minima and negative maxima for the Chi-Chi earthquake for 3 directions of ground motion and simulated accelerograms for varying values of ζ_f.

From (Fig. 2), the cumulative counts of positive minima and negative maxima are similar for the 3 components of ground motion, supporting our initial assumption of a correlation between the directional components. For each ζ_f, each accelerogram will produce a different cumulative count plot. The cumulative counts of positive minima and negative maxima for five different simulations are plotted for each value of ζ_f in (Fig. 2). The plots for different accelerograms with similar ζ_f, however, are similar and overlapping as shown in (Fig. 2). Therefore, one simulation for each ζ_f is sufficient for comparison with the plot from the ground motion to find the best-fit ζ_f. From (Fig. 2), we choose $\zeta_f = 0.25$, which negates the error on either side, compared to $\zeta_f = 0.2$ and $\zeta_f = 0.3$, which underestimate and overestimate the ground

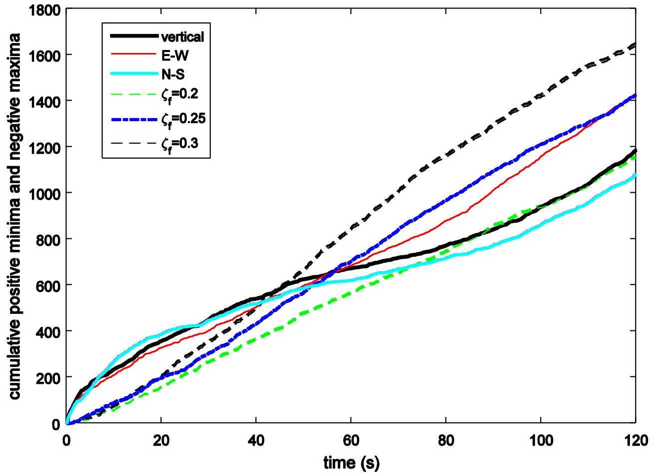

Fig. 2. Characteristics of motion for 3 directional components of ground motion and varying values of ζ_f.

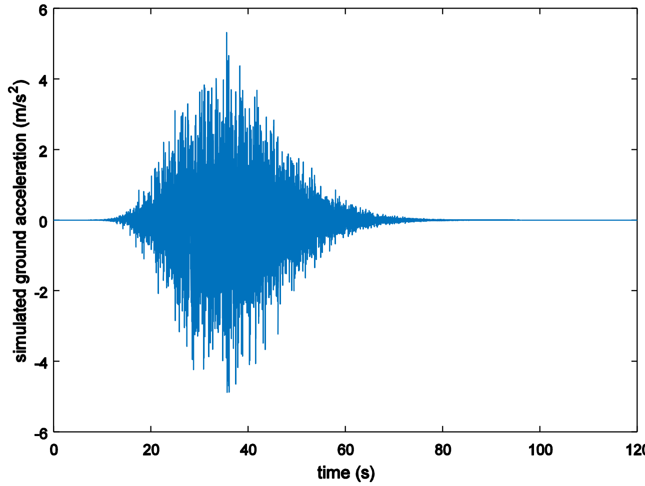

Fig. 4. One realization of simulated ground motion.

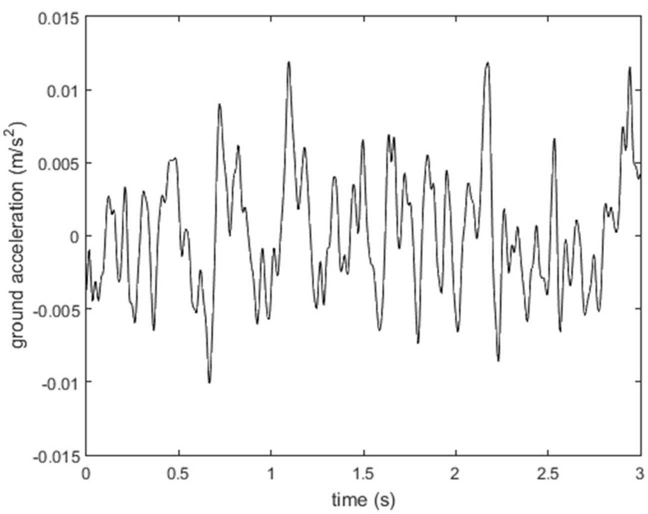

Fig. 3. First 3 s of ground acceleration obtained from sensor measurements.

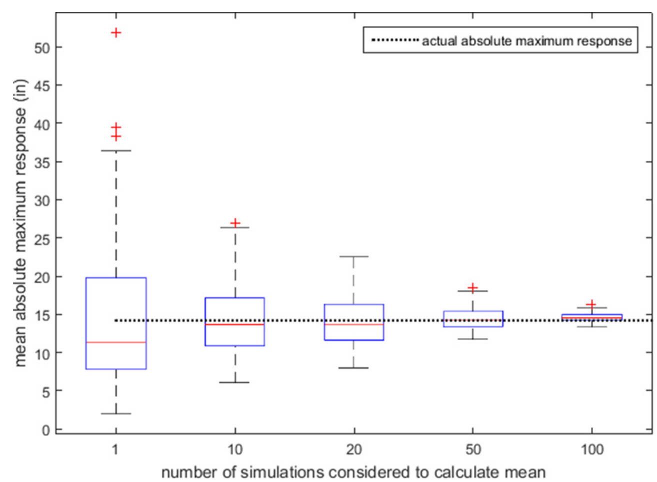

Fig. 5. Distribution of mean maximum response with varying number of simulations.

motion plot, respectively. ζ_f is assumed to be constant and characteristic of the site location, calculated beforehand from any previous recording of ground motion at the site. Robustness of the proposed methodology to errors in the estimation of ζ_f is investigated later in this section.

Fig. 3 shows an example of the separated ground acceleration in the first 3 s based on the structural sensor measurements. This data is used to identify the earthquake parameters as described in Section 3. From these, we then simulate 100 realizations of the ground motion, one of which is shown in (Fig. 4).

Under each ground motion simulation, we calculate the absolute maximum response of the structure using Eq. (4). The predicted maximum response is then estimated as the mean of the results. This predicted maximum from the first 3 s of p-wave data is compared to the actual maximum response of the structure given the full ground motion record to assess the accuracy of the methodology.

4.2. Estimation accuracy and number of simulations

Fig. 5 shows the variation in the accuracy of the methodology as a function of the number of ground motion simulations used for prediction. Each box plot is the result for 100 runs, each using the number of simulations indicated to calculate the mean maximum response. For each box plot, the box represents the 25th to 75th percentile of predicted responses, the central line within the box indicates the median, and outliers are indicated as crosses. The actual absolute maximum response from the full ground motion is also shown.

In (Fig. 5), the estimated mean maximum response converges to the actual maximum response with an increasing number of simulations. The spread of the predicted maximum response also decreases. The estimated mean converges to a value slightly higher than the actual absolute maximum response due to the conservative approach taken in the ground motion simulation process as described in Section 3.

Fig. 6 shows the variation of the root mean square (RMS) error for the maximum response and the total simulation time required to run the methodology for varying numbers of simulations.

In (Fig. 6), we see that increasing the number of simulations decreases the error in the prediction. However, the cost of computation increases, as measured by the simulation time. The RMS error using 100 simulations is 3.17% of the actual maximum response compared to an error of 55.33% for a single realization. The time taken for 100 simulations is 1.79 s compared to 0.033 s for a single simulation. Looking at the trends of the two plots,

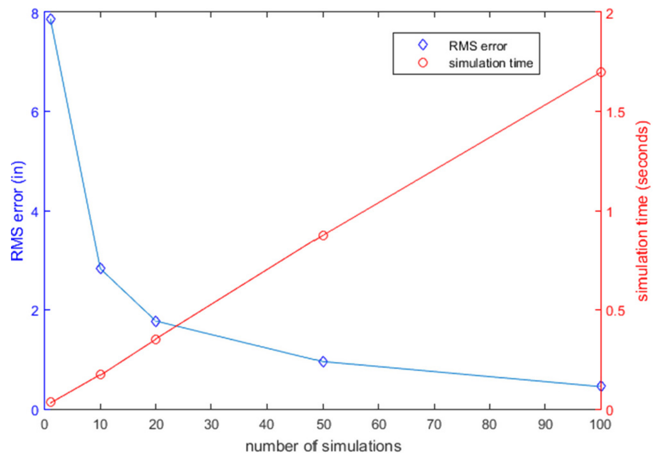

Fig. 6. RMS error and simulation time vs. number of simulations.

the RMS error decreases exponentially, while the simulation time increases linearly as the number of simulations used in the prediction increases. As the RMS error decreases with more simulations, but eventually levels off, whereas the time taken continues to increase, using 100 realizations offers a reasonable tradeoff between accuracy and computational time. In addition, 1.78 s of processing time from an initial 3 s of data is an acceptable time for an earthquake early warning system, particularly considering full ground motion durations of 100–150 s. Hereafter, 100 simulations of the ground motion are used for the results presented in this study.

4.3. Probabilistic inference on structural risk

Fig. 7 shows that the distribution of the predicted maximum response follows closely the lognormal distribution. The mean and standard deviations of the fitted lognormal probability density function (PDF) are within 1% of the mean and standard deviations of the realizations. The fit is shown in the cumulative distribution function (CDF) given in (Fig. 8) as well, which plots the CDF of the realizations compared to the CDF for a fitted lognormal distribution. The highlighted boxed values are probabilities of not exceeding the actual (14.21 in) and estimated mean (14.81 in) maximum

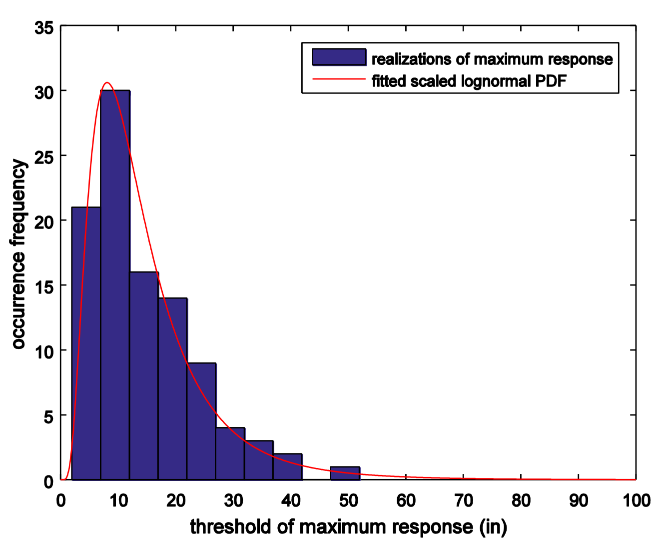

Fig. 7. Distribution of simulated maximum responses and fitted lognormal PDF.

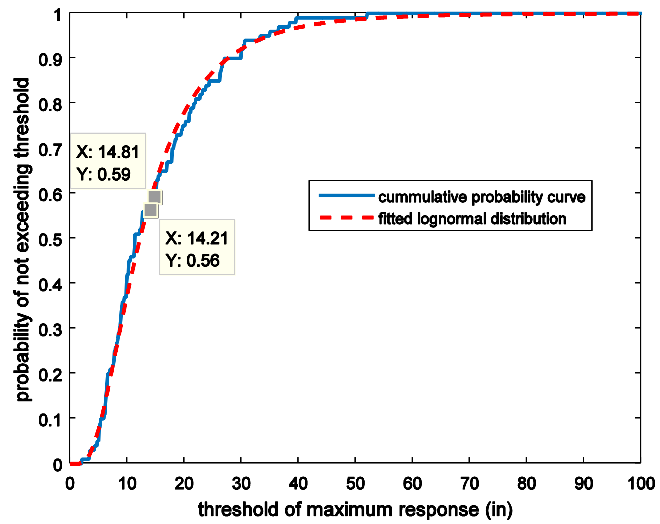

Fig. 8. Cumulative probability of simulated maximum response and fitted lognormal CDF.

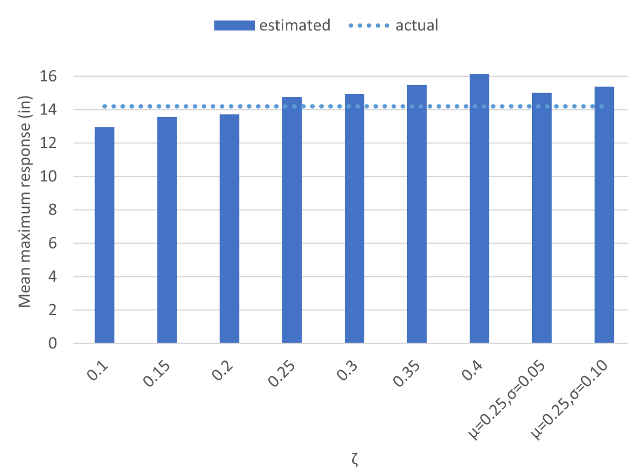

Fig. 9. Variation of mean maximum response with varying ground damping coefficient ζ_f.

responses. Due to the conservative approach, there is a lower probability of exceedance for the estimated response. From (Fig. 7) and (Fig. 8), we see that a lognormal distribution can be used to estimate the probability of exceeding the safe threshold of a structure. Calculating the probability of exceedance can be used to make inferences on the level of risk for a structure under a particular earthquake event, resulting in a warning being issued or the decision for preemptive shutdown of elevators or gas lines.

4.4. Robustness to errors in estimation of ground parameters

In Section 3, we described estimating the value of ground damping parameter ζ_f using the cumulative count of positive minima and negative maxima for the recorded ground motion compared to simulated accelerograms. We propose estimating ζ_f beforehand from previous recordings of ground motions at the site and with the calculated value taken as a constant site parameter. Hence, ζ_f is only a function of the site and independent of other parameters. This assumption, however, introduces potential errors into the methodology. Here, we investigate the performance of the methodology given errors in the estimation of the parameter ζ_f. In (Fig. 9), we show the predicted maximum response compared to the actual response for varying values of ζ_f from 0.10 to 0.40 in steps of 0.05, as well as for parameter values randomized normally with mean 0.25 and standard deviations 0.05 and 0.10. 100 realizations of the ground motion are used to calculate the mean absolute maximum response for each case.

Fig. 9 shows the variation of the predicted mean maximum response for different values of ζ_f. We see that though the error increases with increasing error in estimation of ζ_f, the predicted response is within 10% of the actual response, on either side of the values of $\zeta_f = 0.25$. Additionally, the prediction shows a consistent trend over the range of ζ_f, and the two cases of randomized parameter values correspond well with the case of a deterministic $\zeta_f = 0.25$.

4.5. Robustness to uncertainty in structural parameters

The proposed methodology requires input structural parameters to calculate the structural response for each realization of ground motion. Structural parameters are typically estimated or modeled, for example, based on design drawings. There is uncertainty in this estimation, however. In the analyses thus far, we have used the assumed nominal values of the structural parameters. It is important to also assess the performance of the proposed methodology under the case of varying structural parameters subject to uncertainty. To do this, we lognormally vary the mass m, stiffness k, and damping c of the structure over a range of coefficients of variation (c.o.v.) and means as the nominal values. Fig. 10 shows the estimation results for c.o.v. of m and k ranging from 0% to 20% with a step size of 1% and c.o.v. of c varying from 0% to 40% in increments of 2%. For each of the 100 ground motions, we draw 20 and 100 realizations of m, k, and$c$ for each value of c.o.v., and the responses for all 100 ground motion simulations are estimated. The calculated mean of 20 and 100 mean maximum absolute responses at each variation in c.o.v. are shown.

Noting the ordinate scale, Fig. 10 shows the prediction of the maximum response to be robust to uncertainty in the structural parameters. For 20 realizations of m, k, and c, the maximum error is less than 4.5% of the estimated maximum response using the nominal values. For 100 realizations, the maximum error is less than 1.7%. The slight upward trend in the predicted mean maximum response as c.o.v. increases is due to the right skewness of the lognormal distribution. It is noted that a random variation of 20% c.o.v. for m and k and 40% for c is a significant variation from the nominal values. The accuracy of the prediction at such values shows the robustness of the methodology to uncertainty in the estimation of these structural parameters.

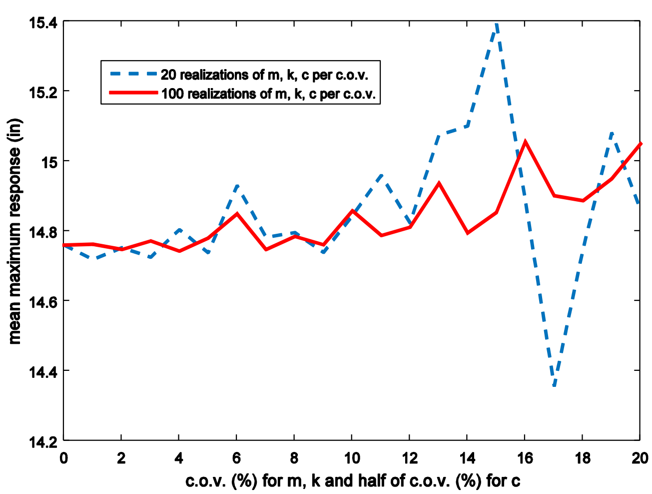

Fig. 10. Variation of mean maximum response with varying m,k, and c.

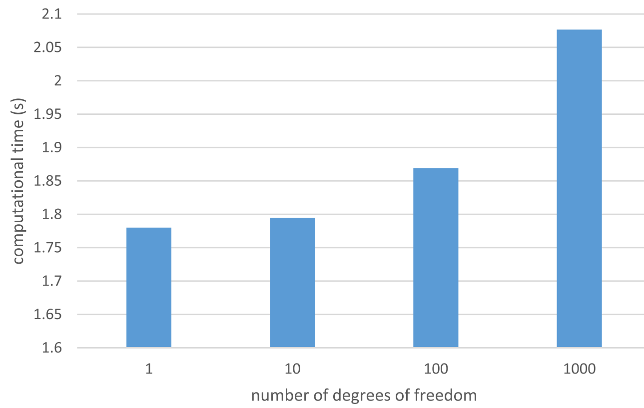

Fig. 11. Computational time vs. number of degrees of freedom of the structure.

4.6. Cost of computation with increasing number of degrees of freedom

We have used a single degree of freedom system to demonstrate the methodology. However, it is also important to analyze the cost effectiveness of the methodology for higher degrees of freedom systems. In (Fig. 11), we compare the computational time required to run the methodology for systems with 1, 10, 100, and 1000 degrees of freedom. We first generate 100 simulations of the ground motion and calculate the response of the system under each of the ground motion realizations. We then calculate the mean of the absolute maximum response at every degree of freedom, which is the predicted maximum response at that degree of freedom.

In (Fig. 11), we see that there is only a slight increase in the computational time as the number of degrees of freedom increases. Specifically, the computational time increases from 1.78 to 2.07 s when increasing from a single to 1000 degrees of freedom system. This is due to the majority of the total time being utilized by the simulation of ground motions. Once we have the 100 ground motion realizations, we are able to calculate the structural response for each realization in parallel. Hence, the computational time is restricted not by the number of degrees of freedom of the system but the number of ground motion realizations. We note that we are using a sampling time of 0.004 s, corresponding to a sampling frequency of 250 Hz. This is equal to the sampling frequency of the accelerometer used to record the data for the Chi-Chi earthquake. If the sampling frequency is higher, then the computational time will be higher. A higher sampling frequency, however, provides more information, resulting in more accurate estimations. Hence, there is a tradeoff between accuracy and computational time for varying accelerometer sampling frequency. It is also noted that for practical structures, we can compress the actual system to use a model with fewer degrees of freedom if desired. The increased number of degrees of freedom could also increase the accuracy of prediction based on sensor placement or number of sensors as shown in [28–30].

4.7. Performance of methodology across range of earthquake events

Finally, we investigate the performance of the methodology across a range of earthquake events. These earthquakes are chosen to demonstrate the generalizability of the methodology across geographical locations and fault types. Table 1 provides the earthquake event, data sampling frequency, actual moment magnitude M_w, predicted M_w using the relations described in Section 3, and ground

Table 1
Performance of the methodology for several earthquakes.

Earthquake	Sampling frequency (Hz)	M_w *actual*	M_w predicted	ζ_f	Actual response (in)	Estimated response (in)	Percentage error (%)
Chi-Chi	250.0	7.6	7.3	0.3	14.2	14.8	3.9
British Columbia	200.0	5.6	5.8	0.4	0.7	1.0	37.0
Manjil, Iran	100.0	7.4	6.4	0.2	11.6	12.5	7.8
Alaska	100.0	7.9	7.6	0.2	7.3	8.2	12.4
Chile	100.0	8.2	7.7	0.2	2.7	3.2	18.5
Napa, CA	200.0	6.0	6.2	0.2	8.4	9.2	8.8

damping ratio ζ_f. The next two columns show the actual maximum response of the structure under the full earthquake event and the predicted maximum response using the proposed methodology. The last column shows the percentage error between the actual response and estimated response. From (Table 1), we see that while there is some variation in the accuracy of the estimated response across the earthquake events, the methodology based on the 3 s of initial data from building-mounted accelerometers is able to perform the prediction across a range of magnitudes of the maximum structural response. For smaller responses, the percentage error is larger but the absolute difference is low.

5. Conclusions

The proposed methodology provides an estimation of the maximum response of a structure under an earthquake threat. Based on the predicted maximum, a localized earthquake early warning can be issued. We use information from the first 3 s of data recorded by accelerometers placed sparsely on the structure, rather than extensive seismograph data, to estimate various earthquake parameters for modeling the ground motion. We find 100 ground motion simulations to achieve a reasonable trade-off between estimation accuracy and computation time. The methodology for maximum response prediction is shown to be robust to uncertainties in the estimation of both ground and structural parameters, and applicable across earthquake-prone regions.

We infer the risk to a structure based on the predicted maximum response. However, we can also look at the projected total response of the structure depending on the criteria defined for failure. To show the generalizability of the method, in this study we did not include specific seismic or site information in the calculations. In the case of regions where studies have defined the relationships between various earthquake parameters, for example, studies for the California area on the relationships between moment magnitude, significant duration, and hypocentral distance, that information can be included in the methodology for improved estimates through fewer simulations. Information on fault type and soil class can also be easily incorporated for improved site-specific results.

The methodology for earthquake early warning enables computationally efficient probabilistic inference on the specific structural risk under an earthquake threat rather than issuing a regional warning. The system can be augmented through incorporation of any known seismic information at the site under consideration. However, we have shown that even with a minimalist approach, the information from accelerometers mounted on a structure can be used for real-time response prediction to issue a structure-specific earthquake early warning. The estimated response can be used to issue a warning based on a pre-designated threshold for maximum structural response. As shown in the results, inference on structural risk can be made based on the probability of exceeding a threshold. This predicted response can also be used in active or semi-active stiffness or damping control systems. The methodology reduces the uncertainty inherent in earthquake event and impact estimation to predict localized structural seismic risk.

References

[1] USGS earthquake catalog. Earthquake Lists, Maps, and Statistics, accessed 07/18/2016, http://earthquake.usgs.gov/earthquakes/browse/
[2] Mahsuli M, Haukaas T. Seismic risk analysis with reliability methods, part 1: models. Struct Saf May 2013;42:54–62.
[3] Bonstrom H, Corotis RB. Building portfolio seismic risk assessment using the first-order reliability method. Struct Saf 2015;52(part A):113–120
[4] Ellingwood BR, Kinali K. Quantifying and communicating uncertainty in seismic risk assessment. Struct Saf March 2009;31(2):179–87.
[5] Goulet CA, Haselton CB, Mitrani-Reiser J, Beck JL, Deierlein GG, Porter KA, et al. Evaluation of the seismic performance of a code-conforming reinforced-concrete frame building- from seismic hazard to collapse safety and economic losses. Earthquake Eng Struct Dyn 2007;36:1973–97.
[6] Liel AB, Haselton CB, Deierlein GG, Baker JW. Incorporating modeling uncertainties in the assessment of seismic collapse risk of buildings. Struct Saf March 2009;31(2):197–211.
[7] Pant DR, Constantinou MC, Wijeyewickrema AC. Re-evaluation of equivalent lateral force procedure for prediction of displacement demand in seismically isolated structures. Eng Struct July 2013;52:455–65.
[8] Decó A, Bocchini P, Frangopol DM. A probabilistic approach for the prediction of seismic resilience of bridges. Earthquake Eng Struct Dyn August 2013;42(10):1469–87.
[9] Bozorgnia Y, Bertero VV. Damage spectra: characteristics and applications to seismic risk reduction. J Struct Eng 2003;129(10):1330–40.
[10] Singhal A, Kirmidjian AS. Method for probabilistic evaluation of seismic structural damage. J Struct Eng December 1996;122(12):1459–67.
[11] Nakamura Y. On the urgent earthquake detection and alarm system (UrEDAS). In: Proceedings of 9th World Conference on Earthquake Engineering, Tokyo-Kyoto, Japan, 1988.
[12] Kanamori H. Real-time seismology and earthquake damage mitigation. Annu Rev Earth Planet Sci 2005;33:195–214.
[13] Wu YM, Kanamori H. Experiment on an onsite early warning method for the Taiwan early warning system. Bull Seismol Soc Am 2005;95:347–53.
[14] Wu YM, Kanamori H. Rapid assessment of damaging potential of earthquakes in Taiwan from the beginning of P waves. Bull Seismol Soc Am 2005;95:1181–5.
[15] Wu YM, Kanamori H. Exploring the feasibility of on-site earthquake early warning using close-in records of the 2007 Noto Hanto earthquake. Earth Planets Space 2008;60:155–60.
[16] Wu YM, Kanamori H. Development of an earthquake early warning system using real-time strong motion signals. Sensors 2008;8:1–9.
[17] Allen RM, Kanamori H. The potential for earthquake early warning in southern California. Science 2003;300:786–9.
[18] Olson EL, Allen RM. The deterministic nature of earthquake rupture. Nature 2005;438:212–5.
[19] Wurman G, Allen RM, Lombard P. Toward earthquake early warning in northern California. J Geophys Res 2007;112:B8.
[20] Allen RM. The ElarmS earthquake early warning methodology and its application across California. In: Earthquake Early Warning Syst, Springer, pp. 21–44, 2007
[21] Allen RM, Brown H, Hellweg M, Khainovski O, Lombard P, Neuhauser D. Real-time earthquake detection and hazard assessment by ElarmS across California. Geophys Res Lett 2009;36.
[22] Cua G, Heaton T. The virtual seismologist (VS) method: a Bayesian approach to earthquake early warning, Springer: Berlin Heidelberg, pp. 97–132, 2007
[23] Wu YM, Kanamori H, Allen RM, Hauksson E. Determination of earthquake early warning parameters, τ_c and P_d, for southern California. Geophys J Int 2007;170:711–7.
[24] Shieh JT, Wu YM, Allen RM. A comparison of τ_c and τ_p^{max} for magnitude estimation in earthquake early warning. Geophys Res Lett 2008;35.
[25] Böse M, Hauksson E, Solanki K, Kanamori H, Heaton TH. Real-time testing of the on-site warning algorithm in southern California and its performance during the July 29 2008 M_w 5.4 Chino Hills earthquake. Geophys Res Lett 2009;36.
[26] Böse M, Heaton T, Hauksson E. Rapid estimation of earthquake source and ground-motion parameters for earthquake early warning using data from a single three component broadband or strong-motion sensor. Bull Seismol Soc Am 2012;102–2:738–50.
[27] Cheng MH, Wu S, Heaton TH, Beck JL. Earthquake early warning application to buildings. Eng Struct 2014;60:155–64.

[28] Tien I, Pozzi M, Der Kiureghain A. Inference on maximum structural response based on measured accelerations using dynamic Bayesian network. In: G. Deodatis, B. Ellingwood, and D, Frangopol, eds. Safety, Reliability, Risk and Life-Cycle Performance of Structures and Infrastructures, New York: CRC Press, 2481–2488, June 2013
[29] Saini A, Tien I. Framework for probabilistic assessment of maximum nonlinear structural response based on sensor measurements: discretization and estimation. ASCE J Eng Mech 2017;143(9).
[30] Tien I, Pozzi M, Der Kiureghian A. Probabilistic framework for assessing maximum structural response based on sensor measurements. Struct Saf July 2016;61:43–56.
[31] Esteva L, Rosenblueth E. Espectros de temblores a distancias moderadas y grandes. Boletin Sociedad Mexicana de Ingenieria Sesmica 1964;2:1–18. In Spanish.
[32] Housner G. Engineering Seismology, 1965
[33] Snaebjornsson JT, Sigbjornsson R. The duration characteristics of earthquake ground motions. In: The 14th World Conference on Earthquake Engineering, Beijing, China, 2008.
[34] Hwang H, Lin CK, Yeh YT. Derivation of attenuation relations of Arias intensity using the Chi-Chi earthquake data. In:13th World Conference on Earthquake Engineering, Vancouver, B.C., Paper No. 3108, Canada, 2004.
[35] Wilson RC. Relation of Arias intensity to magnitude and distance in California. U.S. Department of the Interior. U.S. Geological Survey, open-file report 93-556, 1993.
[36] Rezaeian S, Der Kiureghain A. Simulation of synthetic ground motions for specified earthquake and site characteristics. Earthquake Eng Struct Dyn 2014;39:1155–80.
[37] Rezaeian S, Der Kiureghain A. Simulation of orthogonal horizontal ground motion components for specified earthquake and site characteristics. Earthquake Eng Struct Dyn 2011;41:335–53.